

Discovery of an ultra-quantum spin liquid

Y. X. Yang,¹ C. Tan,¹ Z. H. Zhu,¹ J. Zhang,¹ Z. F. Ding,¹ Q. Wu,¹ C. S. Chen¹
T. Shiroka,² D. E. MacLaughlin,³ C. M. Varma,^{4*} L. Shu^{1,5,6*}

¹State Key Laboratory of Surface Physics, Department of Physics,
Fudan University, Shanghai 200433, China

²Laboratory for Muon-Spin Spectroscopy, Paul Scherrer Institut, 5232 Villigen, Switzerland

³Department of Physics and Astronomy, University of California, Riverside, CA 92521, USA

⁴Department of Physics, University of California, Berkeley, CA 94704, USA

⁵Collaborative Innovation Center of Advanced Microstructures, Nanjing 210093, China

⁶Shanghai Research Center for Quantum Sciences, Shanghai 201315, China

*Corresponding author. Email: chandra.varma@ucr.edu (C.M.V.); leishu@fudan.edu.cn (L.S.).

Abstract

Quantum fluctuations are expected to lead to highly entangled spin-liquid states in some two-dimensional spin-1/2 compounds. We have synthesized and measured thermodynamic properties and muon relaxation rates in two related such compounds, one of which is the least disordered of this kind synthesized hitherto and reveals intrinsic properties of a class of spin-liquids. Its measured properties can all be simply characterized by scale invariant time-dependent fluctuations with a single parameter. The specific heat divided by temperature and muon relaxation rates are both temperature independent at low temperatures, followed by a logarithmic decrease with increasing temperature. Even more remarkably, $\sim 57\%$ of the magnetic entropy is missing down to temperatures of $O(10^{-3})$ the exchange energy, independent of magnetic field up to $g\mu_B H > k_B T$. This is evidence that quantum fluctuations lead either to a gigantic specific heat peak from topological singlet excitations below such temperatures, or to an extensively degenerate topological singlet ground state. These results reveal an ultra-quantum state of matter.

The study of quantum fluctuations in interacting matter is of primary interest in physics, encompassing fields as diverse as the thermodynamics of black holes[1, 2], particle physics beyond the standard model[3], the theory of quantum computation[4], and various phenomena

in condensed matter physics. The latter is often paradigmatic, since it allows access and control to a wide variety of experiments, and the concepts often cut across different fields. These range from quantum Hall effects[5] to the quantum criticality that governs high temperature superconductivity[6, 7] to the spin liquid states[8, 9], all of which have been intensively studied in the last three decades. Spin liquids, in particular, have been hard to characterize beyond the fact that quantum fluctuations prevent any conventional order in them. Despite extensive experiments, few precise conclusions about the nature of the ground state and low-lying excitations are available, because the results are almost always dominated by cooperative effects, however interesting, of the impurities[8, 9, 10, 11].

We have synthesized the $S = 1/2$ triangular lattice compounds $\text{Lu}_3\text{Cu}_2\text{Sb}_3\text{O}_{14}$ (LCSO) and $\text{Lu}_3\text{CuZnSb}_3\text{O}_{14}$ (LCZSO), and measured their thermodynamic properties and muon spin relaxation (μSR) rates $\lambda(T)$ down to 16 mK. In LCSO magnetic impurities are estimated to be less than a part in 10^3 and other impurities or defects about a part in 10^2 . There are no signatures in either compound of conventional or spin-glass order, or any other cooperative effects of impurities down to the lowest temperature. However, a 5% concentration of Schottky defects (Cu/Zn site interchange) in LCZSO is shown to change properties from nearly defect-free LCSO very significantly. We believe the high purity of LCSO allows us to unearth the extraordinary intrinsic properties of a class of spin-liquids.

For $T \ll$ the Weiss temperature $\Theta_W \sim 20$ K, the deduced specific heat $C_M = \gamma T$ from magnetic excitations and $\lambda(T)$ are constants [$\lambda(T \rightarrow 0)$ is related to γ^{-1}], followed by logarithmic decreases with increasing temperature. These results are shown to be consistent with scale-invariant magnetic fluctuations. An even more surprising result is that the *measured* magnetic entropy in LCSO, obtained from the specific heat from 100 mK to its saturation at high temperatures, is only about 36% of the total entropy $k_B \ln 2$ per spin-1/2. μSR measurements effectively extend these results down to 16 mK. The *missing* entropy does not change in a mag-

netic field up to 9 T at any temperature up to Θ_W . The implications of these results, discussed later, shed a completely new light on the nature of the ground and excited states of a nearly defect-free spin liquid.

We have also synthesized the isostructural nonmagnetic compound $\text{Lu}_3\text{Zn}_2\text{Sb}_3\text{O}_{14}$ (LZSO). LCSO, LCZSO, and LZSO are variations on the $R_3\text{Zn}_2\text{Sb}_3\text{O}_{14}$ series of compounds (R = rare earth)[12], with R = Lu and Zn completely (LCSO) or half (LCZSO) substituted by Cu. So far only powder samples have been synthesized by solid-state reaction methods. All the physical properties shown below have been reconfirmed on independently grown samples.

The crystal structure, lattice dimensions, and x-ray diffraction (XRD) pattern exhibiting narrow Bragg peaks are shown in Supplementary Information (SI) Sec. I for LCSO. The compounds form alternate parallel kagomé planes of Lu and Sb (SI Figs. S1b and S1d). In all three compounds, Cu^{2+} and/or Zn^{2+} ions sit in the slightly distorted hexagons of the Lu^{3+} and Sb^{5+} kagomé layers. The two layers in LCSO have Cu ions in distinct co-ordinations: tetrahedra of Sb (Cu1) and octahedra of Lu (Cu2). In SI Sec. III we show the results of dc and ac susceptibility measurements down to 0.1 K, estimate the magnetic impurity concentrations, and show evidence of no cooperative effects.

LCSO is extraordinarily defect-free, with less than 10^{-3} “orphan” spins and negligible Schottky defects. Static magnetism, ordered or disordered, would be expected from orphan spins, but μSR experiments rule this out down to ~ 16 mK. LCZSO has alternate planes with primarily Cu in the Lu layers and Zn in the Sb layers. We have not been able to make it with less than 5% substitutional defects, most likely site interchange of Cu and Zn. These are observed in XRD data and give rise to a low-temperature Schottky contribution to the specific heat; they also affect other properties significantly.

In SI Sec. II we discuss the symmetry of the orbitals where the spins reside, which we argue suggests the two-dimensional nature of magnetic interactions in both compounds. Although

the details of the microscopic Hamiltonian are not known, the fact that the magnetic susceptibility, the specific heat and the muon relaxation rate in LCSO can all be separated into two distinct components, each characterized by the same two parameters, implies that the exchange interactions in the two layers interact dominantly only with other ions in the same layer. The slight distortions from equilateral of the triangles will lead to slight variations in the exchange interactions in the spatial directions.

Figure 1a shows the measured zero-field specific heat $C(T)$ in LCSO and LCZSO from 60 mK to about 300 K, as well as that of the isostructural nonmagnetic compound LZSO; the latter allows a very accurate subtraction of the lattice contribution C_{latt} . A weak bump in $C(T)$ at about 1 K and an increase below 0.2 K can be seen in both compounds. The low-temperature increase is the expected nuclear Schottky contribution (from quadrupolar splitting in zero applied field) $\propto T^{-2}$, which can be isolated from the bump because the latter is negligible compared to the former at low temperatures. We have carefully investigated the bump. The variation of both the low-temperature increase and the bump with magnetic field are described in SI Sec. IV, where we show that the bump is a Schottky anomaly due to non-magnetic impurities[13] with an excited magnetic state. All of our conclusions are affected by less than 0.5% whether or not we subtract the Schottky contribution.

The magnetic contribution $C_M(T, H)/T$ is deduced from $C_M/T \equiv [C - (C_{\text{latt}} + C_{\text{nuc}} + C_{\text{imp}})]/T$, where C_{nuc} and C_{imp} are the nuclear and impurity Schottky contributions, respectively. $C_M(T, H)/T$ at various fields is shown in Fig. 1b for LCSO and in SI Fig. S7b for LCZSO. For $H = 0$ $C_M(T)/T$ is constant at low temperatures, below about 0.4 K for LCSO and below about 1 K for LCZSO (SI Fig. S7b). There is an approximately logarithmic decrease with increasing temperature at higher temperatures in both compounds. This and other features are examined in detail in SI Sec. VI, where the logarithmic behavior is shown to be characterized by parameters close to the respective Weiss temperatures.

The results of our specific heat and μ SR measurements are central to the conclusions of this work. In low-temperature specific-heat measurements, especially in insulators, one must ensure that thermal equilibrium is reached in the measurements. The steps we have taken to achieve equilibrium and the evidence for it are described below in the Methods section.

We turn next to the measurable magnetic entropy. Fig. 2a shows the normalized magnetic entropy $[S(T, H) - S(0.1K, H)]/R \ln 2$ calculated by integrating C_M/T from 0.1 K to T . For $H = 0$ it is $\sim 0.36k_B \ln 2$ per spin-1/2 in LCSO at $T = 20$ K. The uncertainty in these numbers is less than 2%. From the proportionality of the μ SR relaxation rate to C_M/T from 16 mK to 4 K (Fig. 3), we infer that the constant C_M/T also continues to at least 16 mK.

The lattice specific heat becomes very large for $T > 20$ K (Fig. 1A), and it is not possible experimentally to obtain the magnetic contribution directly at any higher temperature. In SI Sec. V, we calculate the entropy at $T \approx \Theta_W$ from the high-temperature series expansion for a triangular lattice, and find it be about $0.07k_B \ln 2$ for LCSO. We therefore conclude that either about 57% of the magnetic entropy ($1 - 0.36 - 0.07$) resides in the ground state in LCSO or, more likely, the average C_M/T below ~ 16 mK is about 10^3 times the measured constant value above ~ 100 mK.

At low temperatures the expected decrease $\Delta S_M(T, H) = S_M(T, H) - S_M(T, 0)$ of the entropy with H is observed (Fig. 2a). At temperatures above about 20 K its apparent saturation to a smaller value with field cannot be ascertained accurately by the above subtraction procedure, where as noted above the specific heat is dominated by the lattice contribution. We determine the entropy in a magnetic field by an alternate more accurate method, which also gives an estimate of the accuracy of the subtraction procedure below 20 K.

In the alternate method, the magnetization $M(H, T)$ is measured from 4 K to 300 K at various fields (SI Figs. S4a and S4c). $(\partial M/\partial T)_H$ for both LCSO and LCZSO are given in SI Figs. 4b and 4d. We then use the Maxwell relation $(\partial S/\partial H)_T = (\partial M/\partial T)_H$, and integrate

$(\partial S/\partial H)_T$ to give the change in entropy due to the magnetic field as a function of temperature. The results are displayed as red points in Fig. 2b, where the results from the direct determination by subtraction shown in Fig. 2a are shown as black points. To get a measure of the consistency of results obtained by these quite different methods, we note that the standard deviation of the red and black points in LCSO is 0.02.

The results in Fig. 2b show that the *available* entropy loss due to magnetic fields at low temperatures is systematically recovered asymptotically at higher temperatures to its zero-field value. However, the *missing* entropy is field independent up to 9 T over the whole temperature range. From this behavior at $g\mu_B H \leq k_B T$ it follows that the missing entropy is due to purely singlet excitations. Since it is unaffected even for $g\mu_B H \gg k_B T$ for $k_B T$ larger than the (small) Θ_W , local mutually non-interacting singlet states are also ruled out because their population would be replaced by the doublet states favored by magnetic polarization. We have checked by measuring in a field while both warming and cooling and in cooling in a field and then measuring that the behavior is unchanged; there is no hysteresis. So the phenomena appears not to be due to metastable singlet states.

μ SR is a direct probe of low-energy spin dynamics. We have carried out zero-field (ZF) and longitudinal-field (LF) μ SR measurements from 16 mK to about 20 K in both LCSO and LCZSO, the details of which are discussed in SI Sec. VII. Neither long-range order nor spin freezing were detected down to the lowest temperatures. The ZF dynamic muon spin relaxation rate λ_{ZF} for LCSO is plotted as a function of temperature in Fig. 3. It is essentially constant below about 0.5 K, indicating persistent spin dynamics and a high density of magnetic fluctuations at low temperatures[14, 15]. Also shown is the deduced C_M/T , the temperature dependence of which closely follows that of λ . A temperature-independent relaxation rate as $T \rightarrow 0$ is itself extraordinary. The measured specific heat and its relation to the μ SR relaxation rate suggest a scale-invariant spectral function for magnetic excitations, as discussed below and in SI Sec. X.

We show in the inset in Fig. 3 that the measured $C_M(T)/T$ in LCSO can be separated into two parts for the two layers. The low-temperature constant values for the two layers are approximately inversely proportional to their respective values of Θ_W , and they both decrease logarithmically approximately as $\ln(\Theta_{W1}/T)$ and $\ln(\Theta_{W2}/T)$. The integrated value, i.e. the entropy, is approximately the same for the two layers. These forms only pertain for the ‘quantum region’ below the respective Θ_W ’s. The knee region between the two logarithms requires fit to the semiclassical region $T \gtrsim \Theta_{W2}$. Details are given in SI Sec. VI.

A similar decomposition for LCZSO is given in SI Sec. VIII. Even with only 5% Schottky defects, which are site interchanges of Cu and Zn in the two layers, the ratio of the entropies of the two layers is no smaller than 30%. This emphasizes how important it is to have defect-free compounds to study spin liquids.

Theoretical results for spin liquids and their relation to our experimental findings are summarized in SI Sec. IX. We have not found theoretical results on any relevant model which correspond to the properties discovered here[9, 8].

Both the specific heat and the μ SR relaxation rate $\lambda(T)$ follow from the scale-invariant density of states function $\mathcal{A}_M(\omega, T) = \gamma_M f(\omega/T)$ for magnetic fluctuations proposed in SI Sec. X. Not only is the temperature dependence of $\lambda(T)$ given by this form, but its order of magnitude is obtained from the same coefficient γ_M that reproduces the magnitude of the measured C_M/T . As a function of imaginary time periodic in inverse temperature, $\mathcal{A}_M(\omega, T)$ is equivalent to an algebraic decay $\propto 1/\tau$. A ground-state entropy, which should more accurately be called a temperature-independent entropy, requires a more singular form $\mathcal{A}_0(\omega, T)$, which corresponds to a correlation function of the singlets approximately proportional to $1/\log(\tau)$. This is as quantum as one can get. Some conceptual questions related to this are briefly discussed in SI Sec. X. This form is chosen in the belief that the missing entropy is due to a dynamical effect. The form can be modified easily by introducing a new scale if instead there are equally

unexpected colossal ultra-low energy excitations.

In summary, two related phenomena have been discovered in the nearly defect-free compound LCSO.

(1) Quantitatively related constant C_M/T and μ SR relaxation rates $\lambda(T)$ are observed below a temperature related to the Weiss temperature Θ_W , followed by the same logarithmic cutoff in both measurements. The excitations necessary for these are shown to be scale invariant. They carry finite spin quantum numbers because their entropy for $g\mu_B H \lesssim k_B T$ is systematically reduced due to H ; this leads to constant muon relaxation. They exhaust the *measurable* excitations at all temperatures up to 9 tesla. All measured properties can be related to just the one parameter in the scaling function.

(2) Conclusive evidence is found for *missing* entropy from a colossal density of **singlet** excitations below an ultra-low energy scale compared to the Weiss temperature. Very interesting is also the fact that the ultra-low energy excitations are not removed by a magnetic field as high as 9 Tesla, showing that they are not trivial local singlets but quite probably non-local and topological.

In a close look at the literature (a summary is given in SI Sec. XI), we find that such properties have not been previously observed in any spin-liquid candidates. We think this is because LCSO can be prepared with fewer defects than any other spin liquid investigated so far, so that the intrinsic behavior of a class of spin liquids is revealed. The simplicity and the nature of the singularities in Eqs. (S9)–(S11), with which we can parameterise all the data, invite important new theoretical developments. The magnetic fluctuations suggested by $\mathcal{A}_M(\omega, T)$ should be accessible via neutron scattering. The detection of the scalar excitations $\mathcal{A}_0(\omega, T)$ poses an interesting challenge to experimental techniques. Having no charge or magnetic moment, they are a form of dark matter not observable by the usual spectroscopic techniques.

Methods

0.1 Sample growth and characterization.

We have synthesized the compound $\text{Lu}_3\text{Cu}_2\text{Sb}_3\text{O}_{14}$ (LCSO) by the solid state reaction method. Stoichiometric amounts of Lu_2O_3 , CuO and Sb_2O_3 were thoroughly mixed using an agate mortar, and heated to 1030°C for 60 hours with intermediate regrinding and reheating. So far only powder samples could be synthesized. The crystal structure was determined from powder X-ray diffraction (XRD) data taken at room temperature using a Bruker D8 advance XRD spectrometer ($\lambda = 1.5418 \text{ \AA}$). Rietveld refinement of the X-ray data was made using the GSAS program[16].

LCSO belongs to the rhombohedral pyrochlore family[12, 17], in which kagomé lattices are formed by alternating layers of filled-shell ($S = 0$) Sb^{5+} and Lu^{3+} ions. The spin-1/2 Cu^{2+} ions sit at the centers of the kagomé hexagons (Cu1-Sb and Cu2-Lu). To determine whether the observed properties are specific to the 2D layers, we have also synthesized the related compound $\text{Lu}_3\text{CuZnSb}_3\text{O}_{14}$ (LCZSO), in which nonmagnetic layers, where $S = 0$ Zn ions replace Cu1 and alternate with Cu2 layers. We have been unable to synthesize this compound with less than $\sim 5\%$ site-interchange disorder, despite efforts with different growth protocols.

0.2 Magnetic susceptibility measurements.

DC magnetic susceptibility measurements above 2 K were made using a Magnetic Property Measurement System (MPMS, Quantum Design). The AC magnetic susceptibility was measured over the temperature range 0.1 K–4 K in a Physical Property Measurement System (PPMS, Quantum Design) equipped with AC susceptibility and dilution refrigerator options. The AC susceptibility measurements covered the frequency range from 631 Hz to 10000 Hz.

0.3 Specific heat measurements.

Specific heats were measured by the adiabatic relaxation method, using a PPMS equipped with a dilution refrigerator. Data were taken at temperatures between 50 mK and 300 K for LCSO and LCZSO, and 0.2 K–300 K for the isostructural nonmagnetic compound $\text{Lu}_3\text{Zn}_2\text{Sb}_3\text{O}_{14}$ (LZSO). We took special care to ensure that thermal equilibrium was achieved for the low-temperature measurements. As an example, at base temperature (~ 50 mK), the measurement took 70 minutes. The specified PPMS thermal coupling factor between the sample and sample platform was 95% at 100 mK and 99% for temperatures above 0.6 K. Measurements were made during cooling down to base temperature as well as warming up. Similarly, when measuring the specific heat in a magnetic field, the sample was field-cooled and then measured on warming, and also zero-field cooled, field applied at low temperatures, and then measured during warming. The results were always consistent.

0.4 Muon spin relaxation experiments.

The time-differential μSR technique[18] was used, in which the evolution of the ensemble muon-spin polarization after implantation into the sample is monitored via measurements of the decay positron count-rate asymmetry $A(t)$. μSR experiments were performed down to 16 mK using the DR spectrometer on the M15 beam line at TRIUMF, Vancouver, Canada, and the Dolly spectrometer at the Paul Scherrer Institute, Villigen, Switzerland. Samples were attached to a silver cold-finger sample holder in the DR spectrometer, to ensure good thermal contact with the mixing chamber. Appropriate functional forms of $A(t)$ were fit to the asymmetry data using the MUSRFIT μSR analysis program[19].

Data availability

All data needed to evaluate the conclusions in the paper are present in the main text or the supplementary information.

Acknowledgments

We are grateful to B. Hitti and D. J. Arseneau of TRIUMF and the staff of the Paul Scherrer Institute for their valuable help during the μ SR experiments. C.M.V. performed this work while a “Recalled Professor” at UC Berkeley, and wishes to thank the members of the condensed-matter theory group for their hospitality. This research was funded by the National Research and Development Program of China, No. 2016YFA0300503 and No. 2017YFA0303104, the National Natural Science Foundations of China, No. 11774061, and the Shanghai Municipal Science and Technology (Major Project Grant No. 2019SHZDZX01 and No. 20ZR1405300).

Author contributions

Y.X.Y., C.M.V., and L.S. designed the experiments. Y.X.Y. and J.Z. grew the samples. Y.X.Y. carried out X-ray structure refinement and magnetic characterizations. Y.X.Y., Z.H.Z., and Q.W. performed the specific heat measurements. Y.X.Y., C.T., D.E.M., and L.S. carried out the μ SR experiments, with site assistance from T.S. Y.X.Y., L.S. and C.M.V. analyzed the data. C.M.V. provided the theoretical framework. All authors participated in discussion. The manuscript was written by Y.X.Y., L.S., C.M.V., and D.E.M.

Competing interests

The authors declare no competing interests.

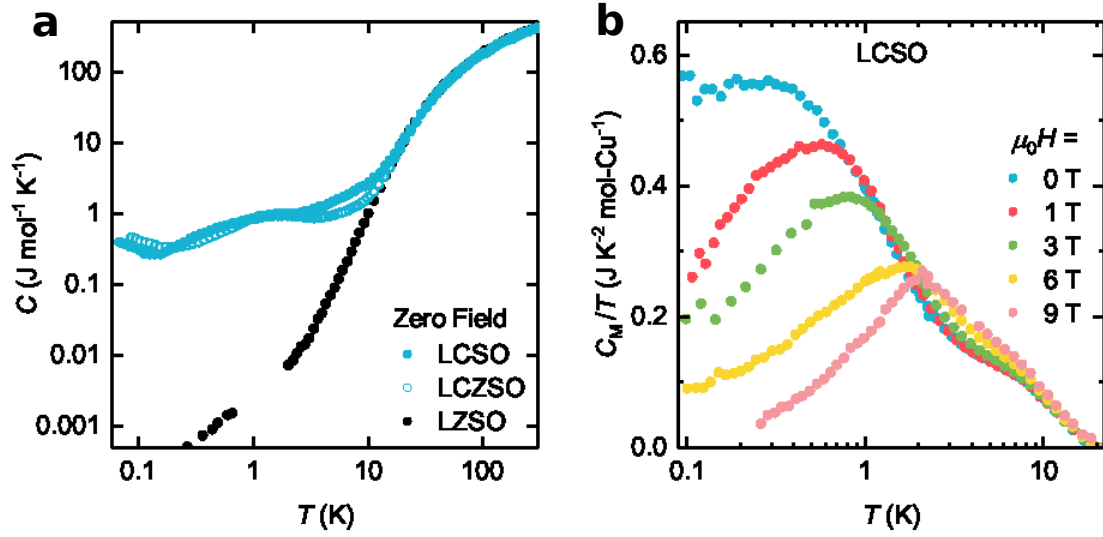


Fig. 1. Specific heat of LCSO, LCZSO, and LZSO. **a**, Measured specific heats in zero field. **b**, Intrinsic magnetic contribution $C_M(T, H)/T$ to the specific heat divided by temperature at various magnetic fields for LCSO, after subtraction of the lattice, nuclear-Schottky, and impurity-Schottky contributions (See text and SI Sec. IV).

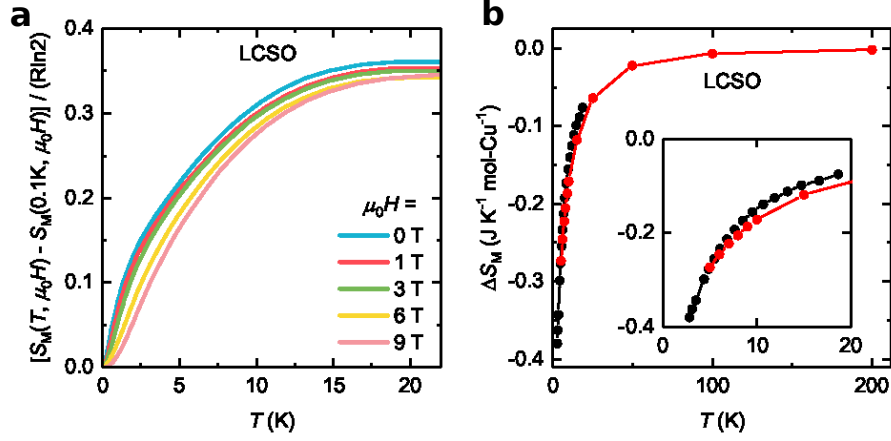


Fig. 2. Entropy of LCSO. **a**, Change $S_M(T, H) - S_M(0.1 \text{ K}, H)$ in magnetic entropy, normalized to $R \ln 2$ per spin, $0.1 \text{ K} \leq T \leq 23 \text{ K}$, $0 \leq H \leq 9 \text{ T}$. **b**, Red symbols: change $\Delta S_M(T, H) = S_M(T, H) - S_M(T, 0)$ in magnetic entropy in an applied field of 9 Tesla as a function of temperature from 2 K to 300 K from measurements of magnetization in LCSO (see text and SI Sec. IV). Black symbols: the same quantity up to 20 K from the direct determination of magnetic entropy shown in Panel **a**. The lost magnetic entropy is fully recovered at high temperatures, proving that the missing entropy is independent of the applied field.

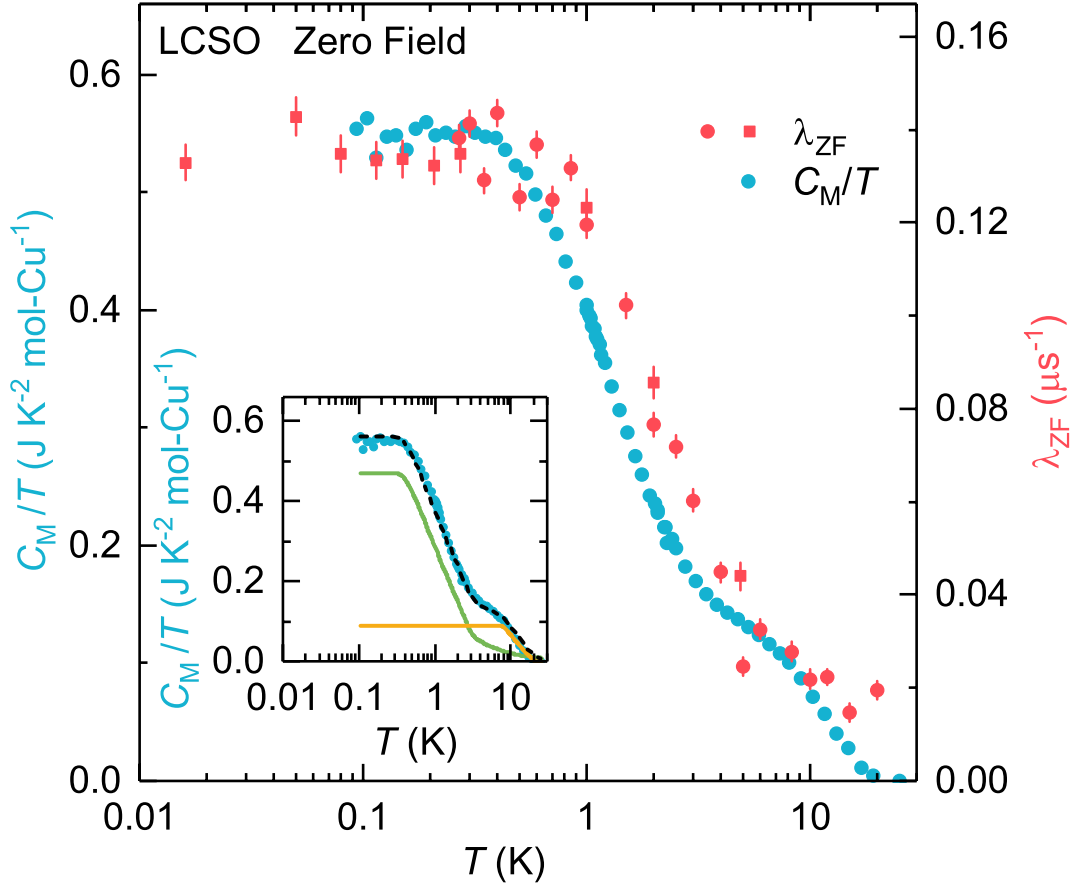


Fig. 3. Muon spin relaxation rate and specific heat in LCSO. A. Temperature dependencies of zero-field muon spin relaxation rate $\lambda(T)$ (red dots: data taken at PSI; red squares: data taken at TRIUMF) and $C_M(T)/T$ (blue dots) at zero field. It is remarkable that the relaxation rate tends to a constant value at low temperatures, and that it follows the temperature dependence of C_M/T over the entire temperature range. Inset: separation of C_M/T into contributions from the two layers (SI Sec. VI). The low-temperature constant values are approximately inversely as their respective Θ_W 's as determined by the fit to the magnetic susceptibility measurements (SI Sec. VI). The characteristic temperatures of the two logarithmic terms are also similar to the respective Θ_W values. The knee between the two logarithms, for $T \gtrsim \Theta_{W2}$ requires a

semiclassical form, which we fit to the expression mandated for $T \gg \Theta_W$. With this fit, the *measured* magnetic entropy is consistent with being the same for both layers.

Supplementary Information: Discovery of an ultra-quantum spin liquid

1 Sample characterization

Figure S1 shows the XRD powder pattern for LCSO, together with details of the crystal structure.

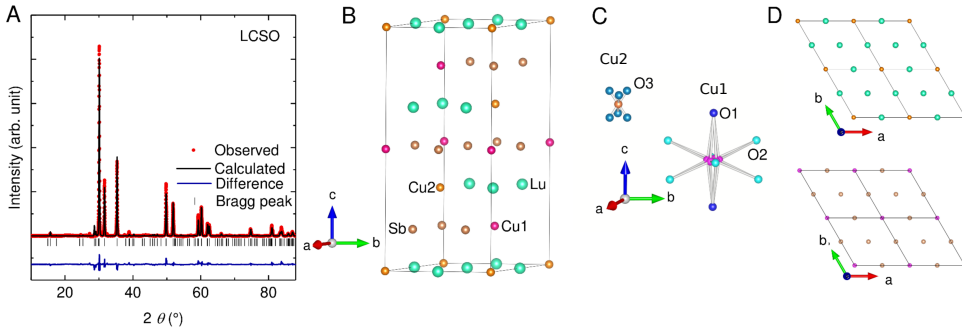


Fig. S1. Rietveld refinement of XRD data for LCSO. **a**, Powder XRD pattern. Red points, black line, and blue line: experimental data, calculated patterns, and residuals, respectively. Black bars: Bragg reflections. **b**, Unit cell. **c**, Inequivalent Cu1 and Cu2 environments. **d**, Inequivalent triangular lattices formed by the spin-1/2 Cu^{2+} ions in the ab plane.

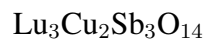
Table S1 lists the fitted values of the structure parameters. In LCSO, inequivalent Cu1 and Cu2 sites form two sets of triangular lattices surrounded by Sb and Lu atoms, respectively. According to the XRD refinement results, Cu1 ions are displaced from the center $3b$ sites $(0, 0, 0.5)$ and located at $18g$ sites $(x, 0, 0.5)$ with a partial site occupation of $1/6$. Such a slight distortion of the Cu1 position (the refined value of x is 0.0505) is consistent with previous work [12, 17].

In LCZSO, $\sim 5\%$ Cu2 sites on the Cu-Lu layer are occupied by Zn ions, and $\sim 5\%$ Zn sites on Zn-Sb layer are occupied by Cu1 ions. We show below that a $\sim 5\%$ impurity level is consistent with the analysis of the impurity Schottky specific heat.

2 Coordination of Cu²⁺ ions and the symmetry of the orbitals

From the detailed structure analysis and the Rietveld refinement, one finds that the Cu²⁺ in the Lu layers are tetrahedrally coordinated and those in the Sb layers are octahedrally coordinated by the O²⁻ ions (see structure in Fig. S1B–D). The tetrahedra do not appear to be distorted, but the octahedral axis perpendicular to the Cu layers is elongated.

Table SI. Rietveld XRD fitting results.

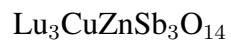


$a = b = 7.322 \text{ \AA}; c = 16.963 \text{ \AA}$

$\alpha = \beta = 90^\circ; \gamma = 120^\circ$

Space Group: $R\text{-}3m$

Atom	Wyckoff positions	x	y	z	Occ.
Sb	9d	0.5	0	0.5	1
Cu1	18g	0.0505(4)	0	0.5	0.1667
Cu2	3a	0	0	0	1
Cu2 (disorder)	9e	0.5	0	0	0
Lu	9e	0.5	0	0	1
Lu (disorder)	3a	0	0	0	0
O1	6c	0	0	0.3922(7)	1
O2	18h	0.4838(2)	-0.4838(2)	0.1308(4)	1
O3	18h	0.0299(5)	-0.0299(5)	-0.0274(1)	1



$a = b = 7.324 \text{ \AA}; c = 16.929 \text{ \AA}$

$\alpha = \beta = 90^\circ; \gamma = 120^\circ$

Space Group: $R\text{-}3m$

Atom	Wyckoff positions	x	y	z	Occ.
Sb	9d	0.5	0	0.5	1
Cu1	18g	0.0320(1)	0	0.5	0.0083
Zn1	18g	0.0401(4)	0	0.5	0.1584
Cu2	3a	0	0	0	0.95
Zn2	3a	0	0	0	0.05
Lu	9e	0.5	0	0	1
Lu (disorder)	3a	0	0	0	0
O1	6c	0	0	0.5359(4)	1
O2	18h	0.5016(1)	-0.5016(1)	0.1231(8)	1
O3	18h	0.3087(2)	-0.3087(2)	-0.3267(1)	1

In an ideal tetrahedral crystal field, the xy , yz and zx orbitals are higher in energy and degenerate. Their linear combinations form bonds with the oxygen. The Cu^{2+} d holes then sit in these linear combinations. In an ideal octahedral crystal field, the levels are reversed and the higher energy states are the degenerate $d_{x^2-y^2}$ and $d_{3z^2-r^2}$ orbitals. Due to the elongation of the octahedra, there is a further splitting so that $d_{3z^2-r^2}$ is the half occupied highest orbital. Moreover, in LCSO the Cu ions in the Sb layers sit in the center of the triangles formed by the Cu in the Lu layers, each of which has orbitals with four-fold phase variation. The exchange integral between the Cu^{2+} ions in different layers would then be zero.

This suggests that in LCSO, where the intralayer distance between Cu sites is shorter than the interlayer distance, the interaction between layers is weak. Therefore LCSO has similar properties per Cu ion as LCZSO, where Cu ions only occupy the Lu layer. We expect that both are two-dimensional as far as the magnetic interactions between the spin-1/2 Cu^{2+} ions are concerned. These arguments are only suggestive, however, and more evidence, e.g. from measurements of crystal-field levels in single crystals, would be required to substantiate them as well as to learn about effects on the levels due to other small distortions of the octahedra.

3 Magnetic susceptibility measurements

Fig. S2A shows the measured inverse DC susceptibility from 2 K upwards for both LCSO and LCZSO. The former exhibits a low-field Weiss temperature Θ_W of 4.4K and $\mu_{\text{eff}} = 1.85 \mu_B$, consistent with a weakly-perturbed free Cu^{2+} ion. In Sec. 6 below we show that in LCSO the susceptibility is best fit by two Curie-Weiss laws of equal amplitude, with $\mu_{\text{eff}} \approx 1.85\mu_B$ and Weiss temperatures 4.37 K and 26.9 K. We also tried to estimate the impurity density by adding a Curie law ($\Theta_W \approx 0$, appropriate to nearly-free impurity spins) and readjusting the Weiss temperatures. Equally good fits are found with an impurity concentration of $O(5 \times 10^{-3})$.

Much stronger estimates of impurity concentrations are obtained from the real part χ'_{ac} of the AC susceptibility measured over the temperature range 0.1 K–3 K, shown in Figs. S2B and S2C. By ascribing all the temperature dependence of χ'_{ac} in this temperature range to a Curie law, we find accurate upper limits to the concentrations of free-spin magnetic impurities to be less than about 10^{-3} in LCSO and about twice that value in LCZSO. No frequency dependence is found

up to 10 kHz (only the lowest frequency results are reported in Figs. S2B and S2C). Thus no spin freezing behavior is observed down to 0.1 K. The region where no transition of any kind (including

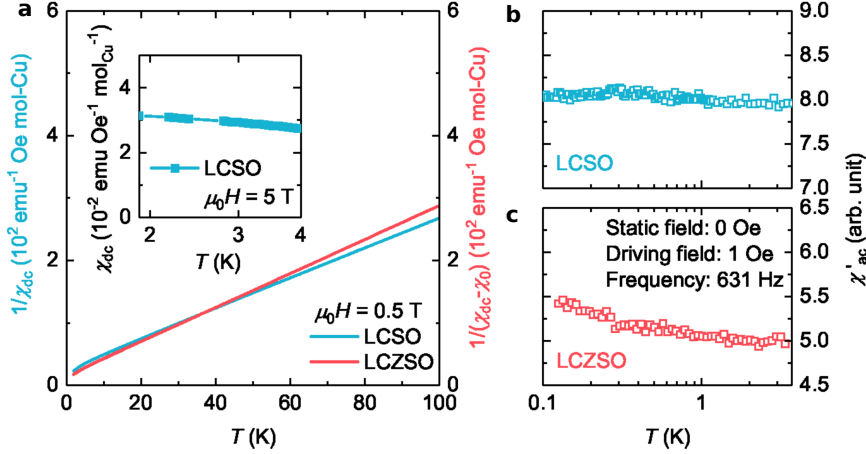


Fig. S2. Magnetic susceptibility. **a**, Temperature dependence of inverse DC magnetic susceptibility $1/\chi_{dc}$ of LCSO and LCZSO. Inset: χ_{dc} of LCSO, $2 \text{ K} \leq T \leq 4 \text{ K}$. A small diamagnetic contribution χ_0 has been subtracted from the data for LCZSO. **b** and **c**, Temperature dependencies of the real part χ'_{ac} of the AC susceptibility in LCSO and LCZSO, respectively, $0.1 \text{ K} \leq T \leq 3.5 \text{ K}$. Similar temperature dependencies were found for frequencies up to 10 kHz. χ'_{ac} , as distinct from χ_{dc} , is not given in absolute units.

a spin-glass transition) could be evidenced from χ'_{ac} is extended down to 16 mK by muon spin relaxation experiments, shown below in Fig. S6.

4 Determination of the magnetic specific heat

The lattice contribution to the specific heat of LCSO and LCZSO can be obtained very accurately from measurement of the specific heat of the nonmagnetic isostructural compound LZSO (main article, Fig. 1A). After subtracting the lattice contribution, the specific heat in both LCSO and LCZSO exhibits a weak bump at about 1 K and an increase below about 0.2 K.

The low-temperature rise is due to the nuclear Schottky contribution $C_{\text{nuc}}(T, H)$, which varies as

$$C_{\text{nuc}}(T, H) = A(H)T^{-2} \quad (\text{S1})$$

for temperatures high compared to the nuclear spin splitting (quadrupolar in zero and low fields). By fitting Eq. (S1) to the rise at the lowest temperatures (where contributions from the lattice and the bump are negligible), the coefficient $A(H)$ could be determined. The nuclear Schottky contributions at various fields and the field dependence of $A(H)$ are shown in Fig. S3A.

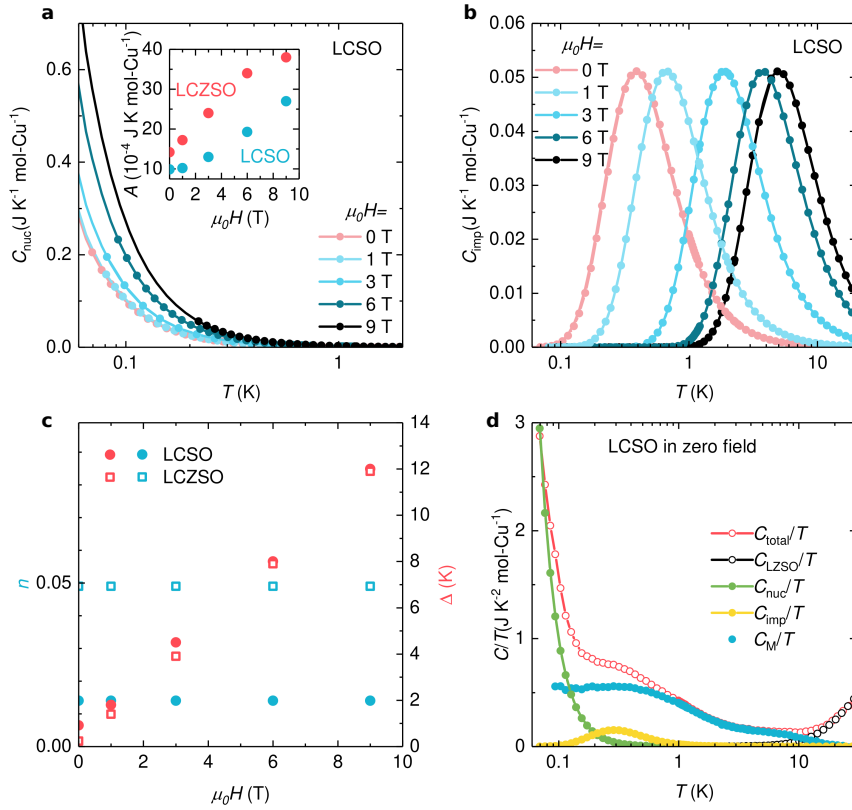


Fig. S3. Nuclear and impurity Schottky specific heats. **a**, Nuclear contribution to specific heat $C_{\text{nuc}} = A(H)/T^2$ at different magnetic fields. Curves: fits of Eq. (S1) to the data. Inset: fitting parameter A for both LCZSO and LCSO. **b**, Impurity Schottky contribution C_{imp} to specific heat at different applied magnetic fields for LCSO. Curves: fits of Eq. (S2) to the data. **c**, Field dependencies of the parameters n and Δ for LCZSO and LCSO from the fits of Panel

B. **d**, Specific heat contributions divided by temperature in LCSO at zero magnetic field. Red: measured total. Black: lattice contribution. Green: nuclear Schottky contribution. Yellow: impurity Schottky contribution. Blue: intrinsic magnetic contribution C_M/T .

The weak bump is hypothesized to be a Schottky contribution due to impurities with non-magnetic ground states. If so, the integrated entropy under the bump should remain constant as the magnetic field is varied, even though the bump may move linearly to higher temperature with increasing field due to excited magnetic states. This hypothesis was tested by using the well-known contribution due to Schottky defects with a concentration n of impurities:

$$C_{\text{imp}}(T) = nR \left(\frac{\Delta}{T} \right)^2 \frac{g_0}{g_1} \frac{\exp(\Delta/T)}{[1 + (g_0/g_1) \exp(\Delta/T)]^2}, \quad (\text{S2})$$

where R is the molar gas constant, Δ is the energy level splitting, and g_0 and g_1 are the degeneracies of the lower and upper levels. Equation (S2) provides a very good fit to the zero-field bump for LCSO with g_0/g_1 set to 1, $\Delta_0 = 1$ K, and $n = 0.014 \pm 0.002$. The area under the bump is field-independent (Fig. S3B)¹. As shown in Fig. S3C, as H is varied n remains constant and Δ increases linearly with H : $\Delta = \Delta_0 + g\mu_B H$, where μ_B is the Bohr magneton and the Landé g factor is found to be 1.3.

In LCZSO, the value of $n = 0.049 \pm 0.02$, which is the same value given for impurities in LCZSO by the Rietveld refinement of the structure (SI Sec. 1). This consistency is strong evidence for the hypothesis of an impurity Schottky contribution. For LCSO n is too small to be determined from the XRD powder pattern.

The intrinsic magnetic contribution $C_M(T)$ to the specific heat is then obtained by subtracting the nuclear contribution $C_{\text{nuc}}(T)$ and the nonmagnetic impurity Schottky contribution $C_{\text{imp}}(T)$ as determined above from the difference of the total specific heat and the lattice contribution. The various contributions at $H = 0$ are separately shown in Fig. S3D. $C_M(T, H)$ for LCSO at various fields is shown in the main article, Fig. 1B, and for LCZSO in Fig. S7B below.

A further test of the consistency of the procedure is to determine the variation of entropy $S(T, H)$ through the measurement of magnetization $M(H, T)$ at various H and T . We use the

¹Note that $\int C(T) d(\ln T) = \int (C/T) dT$

Maxwell relation

$$\left(\frac{\partial S}{\partial H}\right)_T = \left(\frac{\partial M}{\partial T}\right)_H, \quad (\text{S3})$$

and compare $S(T, H)$ obtained by this method with that determined directly from $C_M(T, H)$. $M(H, T)$ and $(\partial M/\partial T)_H$ are shown in Fig. S4, and the deduced changes in entropy for $\mu_0 H = 9$ T are shown in Fig. 2B of the main article. The agreement also provides a quantitative measure of the consistency between the results of these quite different techniques, cf. Figs. 2B and S7D. As discussed in the main article, $S(T, H)$ from the magnetization serves to determine the slow approach at high temperatures of the measured entropy at finite H to its value at $H = 0$.

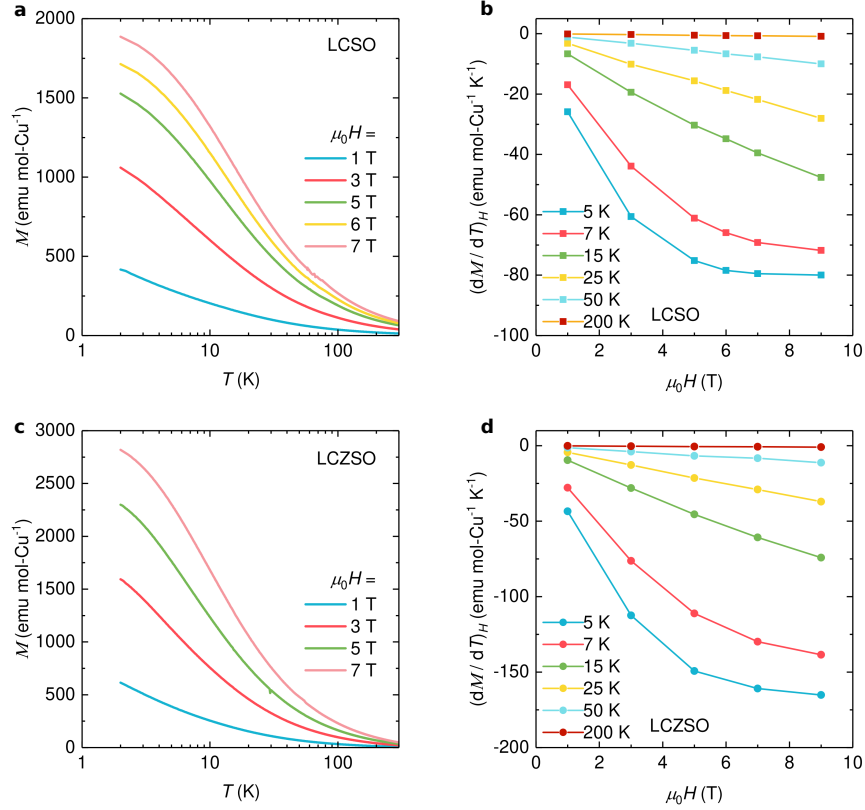


Fig. S4. Magnetization and entropy. **a**, Measured magnetization from 2 K to 300 K for various magnetic fields for LCSO. **b**, $(\partial M/\partial T)_H$ for LCSO at a few selected temperatures as a function of magnetic field. **c** and **d**, As above, for LCZSO. These results are used to obtain the change in entropy with field at various temperatures as shown in the main article, Fig. 2B.

5 High temperature series for a triangular lattice

Above about 20 K, which is close to the higher of the two Weiss temperatures Θ_W in the two layers of LCSO (Sec. 6 below), the lattice heat capacity becomes larger than $10 \text{ J mol}^{-1} \text{ T}^{-1}$ and any magnetic contribution to the specific heat less than a few percent of that value becomes hard to extract. To get a more accurate value of the missing entropy, we use the high-temperature series expansion to estimate the deviation from the asymptotic value $k_B \ln 2$ per spin due to semiclassical fluctuations. High-temperature series expansions to 12th order for

the susceptibility and energy are available for the Heisenberg model on a triangular lattice [20]. One finds $\Theta_W = (3/2)J$ (the coefficient of the Heisenberg interaction) from the leading deviation from the Curie law. The entropy from the leading two terms of the expansion of energy in (J/T) , which is adequate to a percent at $T = \Theta_W$, is

$$S(T) = k_B \left[\ln 2 - \frac{1}{8} \left(\frac{\Theta_W}{T} \right)^2 + \frac{1}{36} \left(\frac{\Theta_W}{T} \right)^3 + \dots \right].$$

The deviation from $k_B \ln 2$ at $T = \Theta_W$ is 14% of $k_B \ln 2$. We should therefore expect that in LCSO, the high temperature un-extracted entropy due to the one layer with $\Theta_W \approx 20\text{K}$ is about 7% of $k_B \ln 2$ per Cu. From Fig. 2A of the main text, the entropy at about 20 K is $0.36 k_B \ln 2$, to which this is added to get the value of the missing entropy to be about 57% of $k_B \ln 2$.

6 Two weakly-interacting Cu sublattices in LCSO

Inequivalent Cu1 and Cu2 sites in LCSO form two triangular sublattices coordinated by Sb atoms and Lu atoms, respectively. Here we present evidence that these two sublattices make additive contributions to the specific heat and the susceptibility.

C_M/T is constant below about 0.6 K in LCSO (main article Fig. 1B) and a similar temperature in LCZSO (see below). A fit of two components to the data for LCSO is shown in the insert to Fig. 3, where each component is constant at low temperatures followed by a logarithmic decrease at higher temperatures [Eqs. (S5) and (S6)].

Quantitatively, for LCSO

$$C_M/T = C_1/T + C_2/T, \quad (\text{S4})$$

where

$$C_1/T \approx \begin{cases} 0.09, & T < 7 \text{ K}, \\ 0.096 \ln(20/T), & T > 8 \text{ K}, \end{cases} \quad (\text{S5})$$

and

$$C_2/T \approx \begin{cases} 0.46, & T < 0.4 \text{ K}, \\ 0.2 \ln(4.2/T), & 0.5 \text{ K} < T < 3 \text{ K}, \\ 0.2/T^3, & T > 3 \text{ K}, \end{cases} \quad (\text{S6})$$

in units $\text{J K}^2 \text{ mol-Cu}^{-1}$.

In the fitting of the specific heat in Fig. 3 and Fig. S7, a knee is observed between the two approximately logarithmic decrease regions. We fit this with the contribution mandatory in the

‘semiclassical’ regime $T \gg \Theta_W$, where $C_M/T = \alpha(1/T)(\Theta_W/T)^2$ and α is a constant that depends on the lattice and number of nearest neighbors.

As shown in Fig. S5A, in LCSO the temperature dependence of the DC magnetic susceptibility χ_{dc} can be fit by a sum of two Curie-Weiss terms with equal weights:

$$\begin{aligned} \chi &= \chi_1 + \chi_2 \\ &= \frac{N_A \mu_{\text{eff}}^2}{3k_B(T - \Theta_{W,1})} + \frac{N_A \mu_{\text{eff}}^2}{3k_B(T - \Theta_{W,2})} \quad (\text{LCSO}), \end{aligned} \quad (\text{S7})$$

with a common value of $\mu_{\text{eff}} = 1.85\mu_B$ and two Weiss temperatures $\Theta_{W,1} = -26.9(3)$ K and $\Theta_{W,2} = -4.37(1)$ K.

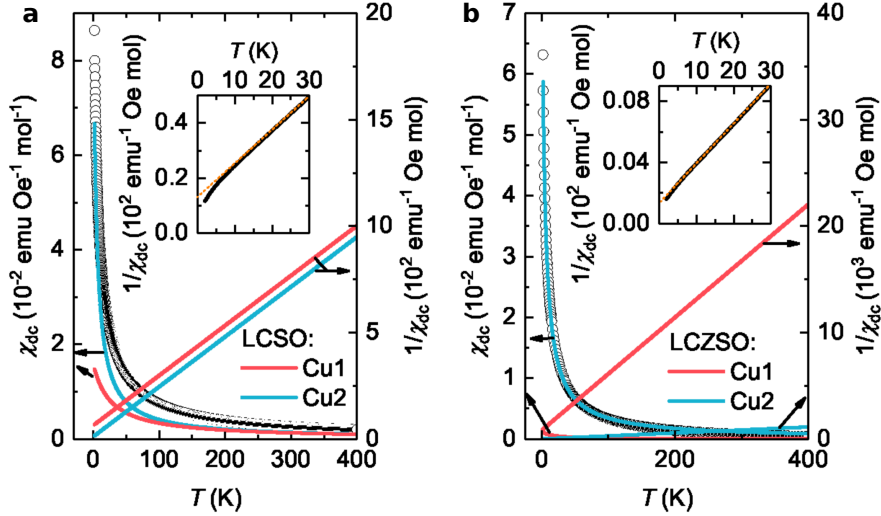


Fig. S5. Two components in susceptibility of LCSO and LCZSO. **a**, DC magnetic susceptibility χ_{dc} of LCSO measured at $\mu_0 H = 0.5$ T (black circles). Curves: two Curie-Weiss dependencies, with the same effective moment and different Weiss temperatures $\Theta_{W,1} = -26.9(3)$ K, $\Theta_{W,2} = -4.37(1)$ K. Inset: inverse $1/\chi_{dc}$ vs T , showing downward curvature at low temperatures. **b**, DC magnetic susceptibility χ_{dc} of LCZSO measured at $\mu_0 H = 0.5$ T (black circles). As in LCSO, two Cu sublattices contribute to the susceptibility of LCZSO, but only $\sim 5\%$ of total susceptibility is from the Cu1 sublattice.

The inset shows the downward curvature of $1/\chi_{dc}$ vs. T that is the signature of a second contri-

bution with a smaller value of Θ_W . We note that the characteristic temperatures in the logarithms in the specific heat [Eqs. (S5 and (S6)] are close to these Weiss temperatures or characteristic exchange energies, and that the ratio of the constant specific heats at low temperature [Eqs. (S5) and (S6)] is approximately the inverse ratio of their respective Θ_W values.

For LCZSO (Fig. S5B), while χ_{dc} can also be fit by a sum of two Curie-Weiss terms, the majority contribution comes from the Cu2 sublattice:

$$\begin{aligned}\chi &= \chi_1 + \chi_2 \\ &= 0.05 \frac{N_A \mu_{\text{eff}}^2}{3k_B(T - \Theta_{W,1})} + 0.95 \frac{N_A \mu_{\text{eff}}^2}{3k_B(T - \Theta_{W,2})} \quad (\text{LCZSO}),\end{aligned}\quad (\text{S8})$$

with a common value of $\mu_{\text{eff}} = 1.73\mu_B$ and two Weiss temperatures $\Theta_{W,1} = -15$ K and $\Theta_{W,2} = -4.0(1)$ K. This is consistent with the observation from XRD that $\sim 5\%$ of Zn sites on Zn-Sb layers are occupied by Cu1 ions (SI Sec. 1). The near equality of $\Theta_{W,2}$ values for the two compounds is evidence that in Eqs. (S7) and (S8) χ_1 and χ_2 are the contributions of the Cu1 and Cu2 layers, respectively.

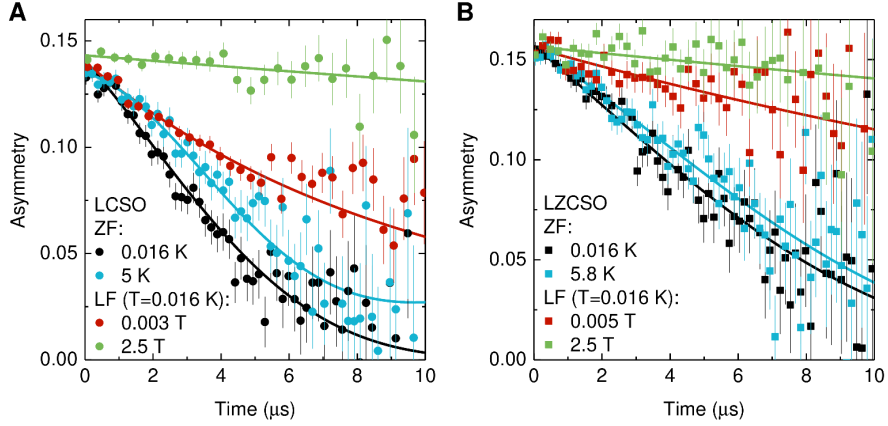
7 Muon spin relaxation

Zero-field (ZF) and longitudinal-field (LF) μ SR experiments were performed over the temperature range 16 mK–20 K. Positive muons implanted in the sample are highly sensitive to the local magnetic fields, with a resolution about 0.1 mT [21].

Representative ZF- μ SR asymmetry spectra are shown in Fig. S6 for both LCSO and LCZSO.

Fig. S6. Zero- and Longitudinal-field μ SR data. Temperature and field dependencies of μ SR asymmetry spectra. **a**, LCSO. **b**, LCZSO. Curves: fits discussed in the text. A constant signal from muons that miss the sample and stop in the sample holder has been subtracted from the data.

No long-range order or spin freezing is observed. This is evidenced by the lack of any spontaneous coherent oscillation or initial asymmetry loss in the ZF spectra [22, 23]. Static spin-glass behavior is also excluded due to the absence of a 1/3 recovery tail of the muon depolarization due to the random distribution of the static fields [24].



The ZF spectra are best described by the functional form

$$A(t) = A_0 \exp(-\lambda_{\text{ZF}} t) G_{\text{ZF}}^{\text{KT}}(\sigma, t), \quad (\text{S7})$$

where A_0 is the initial count-rate asymmetry, which is found to be temperature independent, and

$$G_{\text{ZF}}^{\text{KT}}(\sigma, t) = \frac{1}{3} + \frac{2}{3}(1 - \sigma^2 t^2) \exp\left(-\frac{1}{2}\sigma^2 t^2\right) \quad (\text{S8})$$

is the ZF Kubo-Toyabe (KT) function, expected [25] from a Gaussian distribution of randomly-oriented static or quasistatic nuclear dipolar fields at muon sites. In Eqs. (S7) and (S8) σ/γ_μ is the rms width of this distribution, $\gamma_\mu = 2\pi \times 135.53 \text{ MHz/T}$ is the muon gyromagnetic ratio, and λ_{ZF} is the rate of exponential damping due to dynamic fluctuations of the local Cu^{+2} spins. σ is found to be temperature independent at low temperatures, with $\sigma = 0.146 \mu\text{s}^{-1}$ for LCSO and $\sigma = 0.081 \mu\text{s}^{-1}$ for LCZSO, typical values of the nuclear dipolar field distribution from the host. With decreasing temperature λ gradually increases, saturates below 1K, and remains essentially constant down to the lowest measured temperature of 16 mK for both LCSO (Fig. 3) and LCZSO (Fig. S7A). A phenomenological stretched-exponential function $A(t) = A_0 \exp -(\lambda t)^\beta$ has also been fit to the ZF data. The fits (not shown) are good but with somewhat larger statistical χ^2 values. The temperature dependence of λ is similar to that from fits of Eq. (S7), with temperature-independent $\beta \approx 1.2$.

By applying a longitudinal magnetic field H_L (i.e., along the initial muon spin polarization), $G_{\text{ZF}}^{\text{KT}}(\sigma, t)$ in Eq. (S7) changes to the LF KT form $G_{\text{LF}}^{\text{KT}}(H_L, \sigma, t)$ [25]. Figure S6 also shows

asymmetry spectra for representative values of H_L . When the applied fields are small, the field dependence is dominated by decoupling of the static relaxation. The decoupling is complete at high fields, and the μ SR asymmetry spectra show a single exponential decay. This is evidence that the observed relaxation arises from dynamic spin fluctuations, which persist down to 16 mK. Although the dynamic relaxation becomes slower with increasing magnetic field, it is not completely suppressed even at 2.5 T.

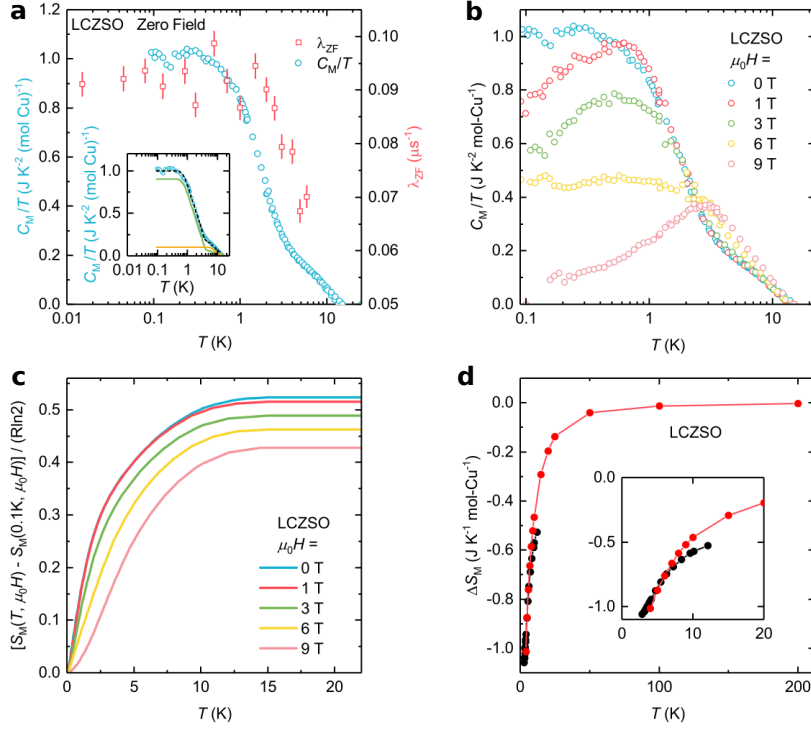
8 Specific heat, Entropy and Muon spin relaxation in LCZSO

The μ SR relaxation rate $\lambda(T)$, specific heat, magnetization, and entropy for LCZSO, shown in Fig. S7A, exhibit the same general behavior as in the purer LCSO (Figs. 1–3 of the main text). In both compounds $C_M(T)/T$ is nearly constant at low temperatures. In LCZSO the fall-off of $\lambda(T)$ occurs at a higher temperature compared to that of C_M/T whereas in LCSO they occur at about the same temperature (main text Fig. 3). The crossover from constant C_M/T to the high-temperature decrease is smoother than in LCSO.

The inset in Fig. S7A shows the partitioning of the specific heat of LCZSO into contributions from the two layers. The ratio of the entropies of the two layers is close to 3:1, although in the ideal case, i.e., without Cu and Zn site interchange, there would be no magnetic entropy in the

Fig. S7. Data for LCZSO. a, Temperature dependencies of the magnetic specific heat divided by temperature C_M/T and the zero-field μ SR relaxation rate $\lambda_{ZF}(T)$. Inset: partition of two components of the specific heat for the two layers in LCZSO deduced in the same way as for LCSO (main text Fig. 3). **b**, C_M/T at the specified magnetic fields. **c**, Magnetic entropy obtained by integrating C_M/T . **d**, Black points: change ΔS_M in entropy in a magnetic field by direct measurement of the specific heat. Red points: from magnetization measurements as described in the text.

Zn layer. The substitution determined by x-ray diffraction and susceptibility measurements is 5% (Sec. 1), but the effect on the entropy is much larger.



9 Theories on relevant spin-liquid models. Ground state entropies.

Detailed numerical calculations [26] on the $S = 1/2$ Heisenberg model on a triangular lattice give an ordered three-sublattice state, with reduction of the order parameter by zero-point fluctuations of about 36% for the nearest-neighbor interaction model. We do not know how the slight distortion of the triangular lattice in these compounds might affect the numerical results for the nearest neighbor Heisenberg model. Numerical calculations on models with substantial next-nearest-neighbor interactions on a triangular lattice [27] have given a quantum-disordered state with gapless excitations conjectured to be *spinons*, but no ground-state entropy or indications of a gigantic peak in exponentially low energy singlet excitations. Spinons have a Fermi surface and therefore a linear-in- T specific heat, but the magnetic fluctuations associated with the Fermi surface lead to a relaxation rate proportional to the density of thermal excitations. It is therefore proportional to T at low temperatures, similar to the Korringa rate in metals and

unlike the constant rate found here.

Calculations on models for ice [28] or spin ice [29] [which agree with experiments [30, 31]], and glass or spin-glass models, possess ground state entropy, but they are obviously inapplicable here. Very careful calculations [32] and analysis of a high-temperature series expansion up to 17th order for $S = 1/2$ Heisenberg spins on a kagomé lattice have found a missing entropy of about 1/2 the total value down to temperatures of $O(J/10)$, the lowest to which the calculations are reliable. The most studied kagomé compound, herbertsmithite [10], has been found experimentally to have scale-invariant magnetic excitations and a specific heat closely related to the form suggested below, but the compound suffers from substantial disorder. No determination of magnetic entropy is available for herbertsmithite, because its nonmagnetic counterpart has not been found.

The only quantum-mechanical models known definitively to give ground-state entropy are models of impurity spins in a metal with parameters tuned to give singularities at $T \rightarrow 0$: the 2-channel Kondo model [33, 34, 35], the two-interacting Kondo-impurity model [36, 37, 38], and mixed-valence impurity models [39, 40]. All these models are supersymmetric at criticality, and have Majorana excitations proportional to the density of *dilute* noninteracting impurities. Holographic field theory models [41, 42, 43] do have ground state entropy as well as observable specific heat with various power laws including linear. (0+1)-dimensional disordered effective-impurity models such as the SYK model [44, 45] also have extensive ground-state entropy as well as gapless fermion excitations giving a linear-in- T specific heat. The mapping of the SYK model to AdS theory of black holes has also been discussed [45]. Black holes are conjectured to be quantum-mechanical and their physics is fashioned parallel to the thermodynamic laws [46]. They are believed to have an observable linear-in- T entropy [1, 47].

10 Specific heat, ground-state entropy, and the muon relaxation rate

The properties reported here can be used to specify some features of the frequency-dependent correlation functions that a fundamental theory might provide. Let us consider only the pure limit and the experimental results for $H = 0$. We show that the *measured* specific heat and

the muon relaxation rate follow if there are magnetic fluctuations with *local* density of states of a specific scale-invariant form, $\mathcal{A}_M(\omega, T)$. The ground state entropy requires a more singular form $\mathcal{A}_0(\omega, T)$.

We write

$$\mathcal{A}_{loc}(\omega, T) \equiv \sum_{\mathbf{q}} \mathcal{A}(\mathbf{q}, \omega, T) \delta(\omega - \omega_{\mathbf{q}}) = \mathcal{A}_0(\omega, T) + \mathcal{A}_M(\omega, T), \quad (\text{S10})$$

where

$$\mathcal{A}_0(\omega, T) = S_0 \frac{\omega}{\omega^2 + T^2} e^{-\omega/T} \quad \text{and} \quad (\text{S11})$$

$$\begin{aligned} \mathcal{A}_M(\omega, T) &= \gamma_M \frac{\omega}{T}, \quad \text{for } \frac{\omega}{T} \ll 1, \\ &= \gamma_M \ln \left(\frac{\omega}{T + T_x} \right), \quad \text{for } T \ll \omega \lesssim T_x. \end{aligned} \quad (\text{S12})$$

Here \mathbf{q} specifies the quantum numbers of the fluctuations, which are different for the two contributions. $\mathcal{A}_M(\omega, T)$, as shown below, provides the measured specific heat $C_M/T \approx (\gamma_M k_B)$ for $T \ll T_x$, and the μ SR relaxation rate, which requires magnetic field fluctuations. $\mathcal{A}_0(\omega, T)$, the local density of states of singlet excitations, can easily be modified if later experiments reveal a gigantic peak in C_M/T at very low temperatures. S_0 and $\gamma_M T$ with a cutoff T_x of order the Weiss temperatures, are related through the sum rule that the total entropy is $k_B \ln 2$ per spin at high temperatures. The fluctuations are assumed to obey Bose-Einstein statistics with zero chemical potential. Were it to turn out that they are hard core bosons or neutral fermions, obvious modifications in the hypotheses above would be required. The possibility that the spectrum represents unfamiliar particles with unfamiliar statistics should also be entertained.

The functional form of $\mathcal{A}_M(\omega, T)$ is derived at criticality in all the impurity models mentioned above, the 2D dissipative quantum xy model [48, 49, 50] and the SYK impurity model [44, 45]. In every case, the low energy excitations in these toy models are topological and so are the $T \rightarrow 0$ states.

The free energy F is given by

$$F = -kT \ln \text{Tr } Z, \quad \text{Tr } Z = \sum_{\lambda} e^{-\beta E_{\lambda}}, \quad (\text{S13})$$

where λ contains the quantum numbers \mathbf{q} as well as their occupation number. Summing over the occupation numbers gives, as usual,

$$\ln \text{Tr } Z = \sum_{\mathbf{q}} \ln \left(\frac{1}{2 \sinh(\beta\omega_{\mathbf{q}}/2)} \right). \quad (\text{S14})$$

Let us first calculate the entropy due to $\mathcal{A}_0(\omega, T)$. One finds the entropy from the free energy [$S = -(\partial F/\partial T)_V$]:

$$S = k_B \frac{d}{dT} T \int d\omega \mathcal{A}_0(\omega, T) \ln \left(\frac{1}{2 \sinh(\beta\omega/2)} \right), \quad (\text{S15})$$

$$= k_B S_0 \left(\int_0^\infty dx x \frac{e^{-x}}{1+x^2} f(x) \right), \quad f(x) = \ln \left(\frac{1}{2} \csc(x/2) \right). \quad (\text{S16})$$

The value of the integral is approximately 0.275.

We briefly comment on the use of the Bose-Einstein distribution with zero chemical potential. The reason this works is that even with zero chemical potential, as can be easily calculated, the number of excitations remains independent of temperature with the choice of the singular density of states of excitations. The divergent damping of the excitations implied by the density of states also obviates a Bose-Einstein condensation. The colossal degenerate fluctuating singlet state is however likely to be unstable to other states by perturbations, for example superconductivity on promoting itinerant charge states by doping.

The local density of states function $\mathcal{A}_M(\omega, T)$ gives a free energy proportional to T^2 with logarithmic corrections at high temperatures, an entropy of the deduced form, and a measurable specific heat

$$C_M(T)/T \approx \gamma_M k_B. \quad (\text{S17})$$

at low temperatures, with a logarithmic cutoff for temperatures above T_x . From the measured value of $C_M(T)/T \approx 0.5 \text{ J/K}^2 \text{ mole}$ at low temperatures, $\gamma_M \approx 3 \times 10^{-11} \text{ s}$. It is noteworthy that its inverse is close to the measured Weiss temperature.

In zero magnetic field, the muon relaxation rate due to magnetic field (dipolar) fluctuations at the muon site given by

$$\lambda(T) = \gamma_\mu^2 \lim_{\omega \rightarrow 0} \frac{T}{\omega} \sum_{\mathbf{q}} |B_{\text{loc}}(\mathbf{q})|^2 \text{Im } \chi(\mathbf{q}, \omega). \quad (\text{S18})$$

where $\text{Im } \chi(\mathbf{q}, \omega)$ is the spectrum of magnetic fluctuations, which summed over \mathbf{q} is identified as $\mathcal{A}_M(\omega, T)$. This is often written as

$$\lambda(T) = \gamma_\mu^2 \langle B_{\text{loc}}^2 \rangle \tau_M(T), \quad (\text{S19})$$

where $\langle B_{\text{loc}}^2 \rangle$ is the mean-square fluctuation of the local magnetic fields at muon sites and $\tau_M(T)$ is the characteristic correlation time of the local field fluctuations [25]. For $\mathcal{A}_M(\omega, T)$ given by Eq. (S12), the temperature dependence of $\lambda(T)$ is seen to be the same as that of C_M/T , as in the experimental results shown in Fig. 3 of the main article. Since $\mathcal{A}(\mathbf{q}, \omega)$ is the absorptive part of the magnetic fluctuation spectra, it follows that at low temperatures $\tau_M \approx \gamma_M$. Quantitatively, from the measured $\lambda(T)$ and the deduced γ_M , we can deduce $\langle B_{\text{loc}}^2 \rangle$ using Eq. (S19). The measured $\lambda \approx 0.1 \mu\text{s}^{-1}$ and $\tau_M \approx \gamma_M \approx 3 \times 10^{-11}$ s, which gives a local rms fluctuating field $\langle B_{\text{loc}}^2 \rangle^{1/2}$ of about 0.1 T. This is roughly the field from $\sim 1\text{-}\mu_B$ moments at a distance of about 4 Å, which is what is to be expected for $S = 1/2$ Cu^{2+} dipolar fields at a typical muon location. Thus the same fluctuations that contribute to the specific heat account semi-quantitatively for the muon relaxation rate.

11 Comparison of properties of LCSO with other putative spin-liquid compounds

Notable experimental discoveries of compounds that do not order (or do not order down to very low temperatures compared to their Θ_W 's) and have been discussed as spin-liquids in the last 25 years. We argue that our results are distinctive, most likely because LCSO is purer than any other compound of this class, so that intrinsic properties of a class of spin-liquids are revealed. Only a representative reference for each compound is given. More complete references may be found in the review [51].

1. Herbertsmithite [52] is a $S = 1/2$ kagomé lattice compound, and has properties closest of any in the literature to those discovered here. C/T and the μSR rate are constant at low temperatures, but no nonmagnetic analog has been made to subtract the lattice specific heat to see if there is an unobservable entropy due to ultra-low energy excitations. It is interesting that single crystals have been made on which neutron scattering reveals a momentum independent

continuum extending down to 0.25 meV, with ω/T scaling proposed here and much earlier in the physics of the cuprates. NMR and μ SR results are similar to those in our compound, except at very low temperatures where evidence for inhomogeneity is found. The compound cannot be made with less than $\sim 5\%$ Zn and Cu site disorder, leading to a Schottky specific heat. This resembles disordered LCZSO rather than ordered LCSO.

2. Some organic Cu compounds, κ -(ET) $_2$ Cu $_2$ (CN) $_3$ [53], EtMe $_3$ Sb[Pd(dmit) $_2$] $_2$ [54, 55] have a linear-in- T contribution to the heat capacity at low temperatures that unlike our results is field independent. Unlike in our samples, it is followed at higher temperatures by a large bump. We have not located any report in the literature of missing entropy or constant NMR rates at low temperatures. In earlier samples a linear-in- T thermal conductivity was observed, but in more recent samples this is not found. The problems and different results in differently prepared samples have been documented in review articles, e.g. [51].

3. Cs $_2$ CuCl $_4$ [56], ZnCu $_3$ (OH) $_6$ Cl $_2$ [57], and BaCo $_2$ (P $_{1-x}$ V $_x$) $_2$ O $_8$ [58] all show ordering of one or the other kind at low temperatures and have Curie contributions to the susceptibility shown by the authors to be due to several percent orphan spins.

4. YbMgGaO $_4$ [59, 60] exhibits a weakly divergent specific heat divided by temperature ($C/T \propto T^{-0.3}$) with $<0.6\%$ residual spin entropy. But a low-temperature Curie tail is observed in the susceptibility, indicative of impurities that are not taken into account in the specific heat analysis. The μ SR relaxation rate is constant below ~ 0.1 K, and does not track C/T .

5. Ba $_3$ CuSb $_2$ O $_9$ [61] has a nominally triangular $S=1/2$ lattice. Entropy saturation to only about $1/3$ of $R \ln 2$ was observed using measurements on a non-magnetic analog to subtract the lattice contribution. But the sample has 5% orphan spins, and a huge peak in the observable specific heat at about 6 K. C_M/T is field independent to 9 Tesla even between 0.2 K and 1 K well below $\mu_B H/k_B$. All this is quite different from the properties of our nearly orphan-spin-free triangular lattice LCSO. Indications are that in Ba $_3$ CuSb $_2$ O $_9$ there is a collective state with glassy ordering at about 6 K, probably induced by non-local effects due to the large concentration of orphan spins.

6. NiGa $_2$ S $_4$ [62] and LCSO have very different properties. Spin freezing is observed in NMR experiments in the former below about 10 K. Relaxation rates have various power laws unrelated to the constant shown in LCSO.

7. TbInO_3 [63] exhibits two distinct Tb ion sites due to a ferroelectric distortion. One forms a triangular lattice. No ordering is seen down to 0.15 K, but other properties do not resemble those in LCSO.

References

- [1] S. Carlip, *Int. J. Mod. Phys. D* **23**, 1430023 (2014).
- [2] J. Maldacena, *arXiv e-prints* p. [arXiv:1810.11492] (2018).
- [3] J. Ellis, *Nucl. Phys. A* **827**, 187c (2009). PANIC08.
- [4] Y. Li, The theory of quantum computation (2016). (unpublished).
- [5] R. Prange, S. E. Girvin, *The Quantum Hall effect* (Springer Verlag, Third Edition, 1990).
- [6] C. M. Varma, *Rep. Prog. Phys.* **79**, 082501 (2016).
- [7] C. M. Varma, *Rev. Mod. Phys.* **92**, 031001 (2020).
- [8] C. Broholm, *et al.*, *Science* **367**, 263 (2020).
- [9] L. Savary, L. Balents, *Rep. Prog. Phys.* **80**, 016502 (2016).
- [10] T.-H. Han, *et al.*, *arXiv e-prints* p. [arXiv:1402.2693] (2014).
- [11] K. Kitagawa, *et al.*, *Nature* **554**, 341 (2018).
- [12] M. B. Sanders, J. W. Krizan, R. J. Cava, *J. Mater. Chem. C* **4**, 541 (2016).
- [13] C. He, *et al.*, *Appl. Phys. Lett.* **94**, 102514 (2009).
- [14] Y. J. Uemura, *et al.*, *Phys. Rev. Lett.* **73**, 3306 (1994).
- [15] Z.-F. Ding, *et al.*, *Phys. Rev. B* **98**, 174404 (2018).
- [16] B. H. Toby, R. B. V. Dreele, *J. Appl. Crystallogr.* **46**, 544 (2013).
- [17] K. Li, *et al.*, *J. Solid State Chem.* **217**, 80 (2014).

- [18] A. Yaouanc, P. Dalmas de Réotier, *Muon Spin Rotation, Relaxation, and Resonance: Applications to Condensed Matter*, International Series of Monographs on Physics (Oxford University Press, New York, 2011).
- [19] A. Suter, B. M. Wojek, *Phys. Procedia* **30**, 69 (2012).
- [20] N. Elstner, R. R. P. Singh, A. P. Young, *Phys. Rev. Lett.* **71**, 1629 (1993).
- [21] A. Amato, *Rev. Mod. Phys.* **69**, 1119 (1997).
- [22] A. Keren, *et al.*, *Phys. Rev. B* **53**, 6451 (1996).
- [23] X. G. Zheng, *et al.*, *Phys. Rev. Lett.* **95**, 057201 (2005).
- [24] Y. J. Uemura, T. Yamazaki, D. R. Harshman, M. Senba, E. J. Ansaldo, *Phys. Rev. B* **31**, 546 (1985).
- [25] R. S. Hayano, *et al.*, *Phys. Rev. B* **20**, 850 (1979).
- [26] F. Mezzacapo, J. I. Cirac, *New J. Phys.* **12**, 103039 (2010).
- [27] S. Hu, W. Zhu, S. Eggert, Y.-C. He, *Phys. Rev. Lett.* **123**, 207203 (2019).
- [28] L. Pauling, *The Nature of the Chemical Bond* (Cornell University Press, Third Edition, 1960).
- [29] P. W. Anderson, *Phys. Rev.* **102**, 1008 (1956).
- [30] W. F. Giaque, J. W. Stout, *J. Am. Chem. Soc.* **58**, 1144 (1936).
- [31] A. P. Ramirez, *Ann. Rev. Mat. Sci.* **24**, 453 (1994).
- [32] G. Misguich, B. Bernu, *Phys. Rev. B* **71**, 014417 (2005).
- [33] P. Nozières, A. Blandin, *J. Phys. France* **41**, 193 (1980).
- [34] I. Affleck, A. W. W. Ludwig, *Phys. Rev. Lett.* **67**, 161 (1991).
- [35] V. J. Emery, S. Kivelson, *Phys. Rev. B* **46**, 10812 (1992).

- [36] B. A. Jones, C. M. Varma, J. W. Wilkins, *Phys. Rev. Lett.* **61**, 2819 (1988).
- [37] I. Affleck, A. W. W. Ludwig, *Phys. Rev. Lett.* **68**, 1046 (1992).
- [38] C. Sire, C. M. Varma, H. R. Krishnamurthy, *Phys. Rev. B* **48**, 13833 (1993).
- [39] I. E. Perakis, C. M. Varma, A. E. Ruckenstein, *Phys. Rev. Lett.* **70**, 3467 (1993).
- [40] C. Sire, C. M. Varma, A. E. Ruckenstein, T. Giamarchi, *Phys. Rev. Lett.* **72**, 2478 (1994).
- [41] T. Faulkner, N. Iqbal, H. Liu, J. McGreevy, D. Vegh, *arXiv e-prints* p. arXiv:1003.1728 (2010).
- [42] K. Jensen, S. Kachru, A. Karch, J. Polchinski, E. Silverstein, *Phys. Rev. D* **84**, 126002 (2011).
- [43] J. Zaanen, K. Schalm, Y.-W. Sun, Y. Liu, *Holographic Duality in Condensed Matter Physics* (Cambridge University Press, 2015).
- [44] S. Sachdev, J. Ye, *Phys. Rev. Lett.* **70**, 3339 (1993).
- [45] A. Kitaev, S. J. Suh, *J. High Energy Phys.* **2018**, 183 (2018).
- [46] J. M. Bardeen, B. Carter, S. W. Hawking, *Comm. Math. Phys.* **31**, 161 (1973).
- [47] J. Maldacena, *arXiv e-prints* p. arXiv:1810.11492 (2018).
- [48] V. Aji, C. M. Varma, *Phys. Rev. Lett.* **99**, 067003 (2007).
- [49] L. Zhu, Y. Chen, C. M. Varma, *Phys. Rev. B* **91**, 205129 (2015).
- [50] C. Hou, C. M. Varma, *Phys. Rev. B* **94**, 201101 (2016).
- [51] L. Savary, L. Balents, *Rep. Prog. Phys.* **80**, 016502 (2016).
- [52] M. R. Norman, *Rev. Mod. Phys.* **88**, 041002 (2016).
- [53] S. Yamashita, *et al.*, *Nature Phys.* **4**, 459 (2008).

- [54] S. Yamashita, T. Yamamoto, Y. Nakazawa, M. Tamura, R. Kato, *Nature Commun.* **2**, 275 (2011).
- [55] J. M. Ni, *et al.*, *Phys. Rev. Lett.* **123**, 247204 (2019).
- [56] R. Coldea, D. A. Tennant, A. M. Tsvelik, Z. Tylczynski, *Phys. Rev. Lett.* **86**, 1335 (2001).
- [57] T. Han, *et al.*, *Nature* **492**, 406 (2012).
- [58] R. Zhong, *et al.*, *Phys. Rev. B* **98**, 220407 (2018).
- [59] Y. Li, *et al.*, *Sci. Rep.* **5**, 16419 (2015).
- [60] Z. Ding, *et al.*, *Phys. Rev. B* **102**, 014428 (2020).
- [61] H. D. Zhou, *et al.*, *Phys. Rev. Lett.* **106**, 147204 (2011).
- [62] H. Takeya, *et al.*, *Phys. Rev. B* **77**, 054429 (2008).
- [63] J. Kim, *et al.*, *Phys. Rev. X* **9**, 031005 (2019).